Supplemental Methods

Mouse experiments

Trans-aortic constriction and micro-osmotic pump placement
All trans-aortic constriction surgeries were performed at the Johns Hopkins Cardiovascular Physiology and Surgery Core by the same operator who was blinded to the genotype or treatments of the mice, as described (1). Mice of both genders, aged between 2-5 months old, were used for these experiments. Mice were anesthetized using isoflurane, intubated and mechanically ventilated at 120 breaths per minute with a tidal volume of 200µl. The aortic arch was approached via a minimal parasternal incision. Once the arch was visible, a small hemoclip (Weck Horizon) was sutured around the transverse aorta, to the diameter of a 27gauge needle, between the innominate artery and the left carotid artery. After the clip was placed, the isoflurane delivery was gradually decreased as the mouse chest wall was closed. The musculature was closed with 5-0 vicryl and skin was closed with 5-0 silk. The isoflurane was then turned off and spontaneous breathing commenced. Within a few minutes, the mouse was extubated. Deaths attributed to a recognized surgical complication (e.g. bleeding, great vessel dissection, failure of intubation) were not censored. Mice were then monitored for death for 4-8 weeks after surgery. Micro-osmotic pumps (Alzet, model 1004) with either KN-93 or KN-92 were implanted subcutaneously two days prior to the TAC surgeries. KN-92 (Millipore Sigma) and KN-93 (Sigma-Aldrich) were dissolved in 50% DMSO and delivered at a dose of 100nM/Kg/day.

Surgically implanted ECG, activity telemeters and echocardiograms
Male mice between 2-3 months of age were used for heart rate monitoring. The mice were anesthetized with isoflurane and a telemeter (DSI model ETA-F10) was implanted in the abdominal subcutaneous area in a lead II configuration. Monitoring and further experiments were performed after at least 5 days of recovery post implantation. Heart rate and activity were monitored for 24 hours. Mice were injected with isoproterenol 0.4mg/kg intraperitoneally, and heart rate was monitored for 30 minutes after injection. The average heart rate 20 minutes prior to isoproterenol injection was used as baseline heart rate for the isoproterenol injection experiments. Heart rate analysis was done using the Ponemah 6.41v software. Transthoracic echocardiography was performed in unsedated mice using a Vevo 2100 (VisualSonics Inc) system, equipped with a 30-40 MHz linear array transducer. The left ventricle end-diastolic and end-systolic ventricular volumes (EDV, ESV), and the percent ejection fraction (EF) were estimated using the Simpson's method from the apical two chamber view of the heart. Measurement of EDV, ESV were manually traced according the American Society of Echocardiography. The echocardiographer was blinded to the genetic identity of the mice for all studies.

Western blots
Mouse hearts were homogenized in 1% triton buffer (10 mM Tris, pH 7.4, 100 mM NaCl, 1 mM EDTA, 1 mM EGTA,10% glycerol) or RIPA buffer with protease (P8340 Sigma) and phosphatase inhibitors (P0044 Sigma). Heart lysates were loaded into 4-12% Tris-Bis NuPAGE gels or 3-8% Tris Acetate Biorad gels (SERCA, RYR). Nitrocellulose or

PVDF membranes were used to transfer proteins using Turbo-blotter (Bio-Rad). Primary antibodies, T287 autophosphorylated CaMKII (Thermo Scientific(MA1047)), CaMKII (Abcam(Ab181052)), GAPDH (Cell Signaling(5174S)), SERCA (Badrilla (A010-20)), RYR (Thermofisher (MA3916)), t-PLN (Cell Signaling (D9W8M)), p-Thr17 PLN (Badrilla (A010-13)) and GAPDH (Invitrogen (PA1-16777)) were incubated with the membrane overnight at 4°C. Secondary antibodies were incubated with the membrane for 1 hour at room temperature. An Odyssey Fc Imager (Licor) was used to image the blots. Bands were quantified using Image Studio Software (Licor).

F-actin staining

Whole left ventricular (LV) free wall tissue from WT, *MICAL1*$^{-/-}$, and *MICAL1*^{R116H} mice were embedded in OTC tissue freezing medium and cryosectioned at 10μm intervals. Sections were fixed in 4% paraformaldehyde in phosphate buffered saline for 10 minutes at room temperature then permeabilized with 0.1% Triton-X for 5 minutes. To assess F-actin, Alexa Fluor 568 Phalloidin (Thermo Fisher Scientific, Waltham, MA USA) staining was performed according to manufacturer's protocol. Samples were excited using an ET490/20x and ET555/20x filter. Emission was collected using an ET525/36m and ET605/52m filter. Immunohistology 0.63 μm Z-stacks were collected using an Olympus IX70 microscope, 40x/0.75NA UPLFLN-PH objective, and deconvolved using constrained iterative deconvolution software in the cellSens software suite. Ten fields of view were acquired across the entire left ventricular free wall of each animal. Four animals were processed per genotype.

Sinoatrial node cell isolation and action potential recordings

Sinoatrial node cardiac pacemaker cells were isolated from adult 8-12 week old, both genders WT and *CaMKII*δ^{M308V} littermates, as described (2). Pacemaker cells were identified by their characteristic appearance and spontaneous activity. The pacemaker cells exhibited spontaneous action potentials with slow depolarization during phase 4, and were included in the experiment only if they had stable, spontaneous action potentials. Pacemaker cell action potentials were recorded at baseline and after isoproterenol treatment (1μM).

Ventricular myocyte isolation and intracellular Ca^{2+} transients

Ventricular myocytes were isolated from adult 7-8 week old, both genders WT and *CaMKII*δ^{M308V} littermates, and WT and *MICAL1*$^{-/-}$ littermates as described (3). Mice were first anesthetized by Avertin intraperitoneal injection (320μg/g/mouse, Alfa Aesar) and after insensibility, the heart was rapidly excised, and placed in iced Ca^{2+} free Hepes-buffered Tyrode's solution. Hearts were retrogradely perfused with a Ca^{2+}-free perfusate for 5 min at 37°C after aortic cannulation. Before the final perfusion with collagenase free-containing low Ca^{2+} (0.2mM) solution, hearts were perfused with collagenase-containing nominally Ca^{2+} free solution for 15 minutes. The left ventricle and septum were cut into small pieces and placed in low Ca^{2+} solution with 1% (w/v) BSA at 37°C. Cardiac ventricular myocytes were dispersed by gentle agitation and collected in serial aliquots where they were maintained in standard saline solution containing 1.8mM Ca^{2+}. Cytosolic Ca^{2+} measurements in isolated myocytes were performed as described (4). Briefly, isolated ventricular myocytes were loaded with 4μM Fura-2 acetoxymethyl (AM)

for 30 min, and subsequently perfused with Tyrode's solution for 30 min to de-esterify the Fura-2 AM. At constant temperature (33 ± 0.5 °C), the cells were perfused in normal Tyrode's solution and stimulated with 1-, 3-, and 5-Hz bipolar pulse using a chamber pacing device (SIU-102, Warner Instruments). SR Ca^{2+} content measurements are peak Ca^{2+} transients induced by perfusion of 20 mM caffeine after 1 Hz stimulation. The cytosolic Ca^{2+} transients were measured from cells excited at wavelengths of 340 and 380nm and imaged with a 510nm long-pass filter.

Drosophila melanogaster experiments

Behavioral circadian rhythmicity assay using beam-break locomotor activity
5-7 day old mated WT and *CaMKII*^{M308V} females were loaded into glass tubes containing 5% sucrose and 2% agarose and were then monitored using the Drosophila Activity Monitoring System (Trikinetics, Waltham, MA) under a 12hr light-12hr dark cycle (LD) for two days before being released into constant darkness (DD) for 8 days. Activity counts, measured as the total number of beam crossings, were collected in 1min bins. Analysis of locomotor activity and circadian parameters was performed using Clocklab (Actimetrics, Wilmette, IL) with circadian period and amplitude estimations performed using the Chi-squared periodogram (5). The circadian rhythm data shown are pooled data from two independent cohorts.

Cardiac physiological analysis of Drosophila melanogaster hearts
Cardiac tubes of 10-day old female WT and *CaMKII*^{M308V} flies (n=30-33) were surgically exposed under oxygenated artificial hemolymph as previously described (6). Briefly, the heads, ventral thoraces, and ventral abdominal cuticles were removed from flies that were anesthetized. The internal organs and abdominal fat were carefully dissected leaving the beating heart. High speed movies of semi-intact *Drosophila* hearts were imaged using a Hamamatsu Orca Flash 2.8 CMOS camera on a Leica DM5000B TL microscope with a 10x immersion lens at ~120 frames per second and analyzed as previously described (7, 8). M-mode kymograms that document the movement of the heart tube edges on the y-axis over time on the x-axis were generated. Myogenic cardiac output was calculated as previously described (9). Significant differences between genotypes were determined using unpaired two-tailed t-tests. When measured values were not normally distributed, data were logarithmically transformed before significance was assessed. Significance was assessed at $p<0.05$.

Ca^{2+}chelation-induced changes in cardiac dimensions
Beating hearts from 10-day old female flies (n=20-23) were imaged as described above using a 20x (0.50 NA) immersion objective lens. Each heart was recorded at various focal depths to resolve clear cardiac edges along the length of the heart tube. After filming beating hearts at baseline, hearts were treated with 10 mM EGTA and 100 µM EGTA-AM (AAT Bioquest) in artificial hemolymph for 30 minutes at room temperature. After Ca^{2+} chelation treatment, the hearts were filmed again at various focal depths. Movies of individual hearts, pre- and post- Ca^{2+} chelation treatment were opened in HCImage Live software and diastolic diameters at baseline and after Ca^{2+} chelation treatment with EGTA were measured as previously described (10). The effect of Ca^{2+}

chelation treatment on cardiac diameters was evaluated using a paired t-test of the means of the matched groups. An unpaired Student's *t*-test was used to identify significant differences in the cardiac response between genotypes. Significance was assessed at $p<0.05$.

Recombinant protein experiments

F-Actin polymerization and depolymerization
To screen MICAL1 mutants for their effects on F-actin depolymerization we used the actin polymerization biochem Kit (fluorescence format) rabbit skeletal muscle actin (Cytoskeleton, Inc.), as described (11, 12). Initially, to polymerize pyrene G-actin to F-actin we diluted pyrene G-actin to 1mg/ml using G-buffer. We then incubated G-actin with the actin polymerization buffer for 1 hour at room temperature, according to the manufacturer's protocol. Pyrene F-actin was then added to 96-well plates. WT and mutant MICAL1 recombinant proteins were added to a final concentration of 300nM. The depolymerization of pyrene F-actin was monitored immediately after the addition of NADPH (200μM), and was apparent by a reduction in the fluorescent signal using an excitation wavelength at 350nm and emission wavelength at 407nm.

Protein preparation for HPLC-mass spectrometry
CaMKII (1μM), with or without MICAL1 (770nM), was incubated for 30 min at room temperature in a total volume of 80 µl of 50mM Hepes, pH 7.4, 20% glycerol, 50mM NaCl, 1.25mM EGTA, 0.5mM DTT, and 2mM NADPH. If not further incubated with MSRA or MSRB, the tube was centrifuged for 1 min at 20,000 *g* after which all of the supernatant was injected onto the HPLC column for analysis. For those tubes that were further incubated with recombinant MSRA or MSRB, 2 µg mouse MSRA or *E.* coli MSRB was added and made 10mM in DTT (Pierce A39255). The tubes were incubated 60 min at 30ºC after which they were centrifuged for 1 min at 20,000 *g* and the entire sample injected onto the HPLC column. For those tubes subjected to tryptic digestion and peptide mapping, DTT was added (10mM) and incubated for 15 min at 30ºCto reduce any disulfide bonds. The solution was made in iodoacetamide (25mM, Sigma I1149) and incubated at room temperature for 15 min in the dark. An additional 5mM DTT was added to scavenge residual iodoacetamide. Modified trypsin (Promega V511A), 50µg, was added and the solution incubated overnight at 37ºC. Peptide mapping was performed as described below.

HPLC-mass spectrometry
Protein separations and mass determinations were performed on a Zorbax 300Å StableBond C18 MicroBore column (1.0 x 50mm, 3.5µm particle size, Agilent 865630-902) with an Agilent 1200 series high pressure liquid chromatography system equipped with a Rheodyne manual injector and a column compartment set to 30°C. The initial solvent was water/0.05% trifluoracetic acid and proteins were eluted by a gradient of 2%/min acetonitrile/0.05% trifluoroacetic acid with a flow rate of 20 µL/min. Effluent from the column was mixed in a tee with 20 µL/min neat acetic acid just prior to the electrospray needle to displace the bound trifluoroacetic acid and generate internal standards (13, 14). Peptide separation and sequencing was carried out as for proteins

except that the gradient was 1%/min from 0 to 45% and an autosampler set to 4°C was used for injections. Electrospray mass spectrometry was performed on an Agilent Model 6520 accurate mass quadrupole-time of flight instrument. Positive electrospray ionization spectra were obtained in the mass range of 100-2500 m/z. The drying gas temperature was 350°C with a flow rate of 10 L/min and a nebulizer pressure of 2 bar. The voltages were capillary 3500V, fragmentor 235V, skimmer 65V, and octopole 1 750V. MS/MS fragmentation used a collision energy of 30 with a data collection range of 20-2000 m/z. Mass spectra were analyzed using Agilent software, MassHunter version B.05. Predicted MS/MS spectra were generated by GPMAW and matched to the experimentally obtained spectra. The sequences were independently confirmed by *de novo* sequencing with PEAKS version 7.0 (Bioinformatics Solutions, Waterloo, ON). The fraction of a tryptic peptide containing Met or MetSO was calculated from the area of the extracted ion chromatograms of the singly charged peptides. Met308 is in the peptide containing residues 302-312 with m/z values for extraction of 1147.650 for the Met peptide and 1163.650 for the MetSO peptide. Met281 and Met282 are in the peptide with residues 276-284, with m/z values for extraction of 1019.476 for the Met peptide and 1035.471 for the MetSO peptide.

CaMKII activity assays

Purified WT and M308V proteins were generated as described above. WT or M308V CaMKIIδ recombinant proteins (1 ng protein) were incubated with 40 μM syntide for 10 min (Hepes 50 mM, pH 7.4, Ca^{2+} 100 μM, EGTA 50 μM, CaM 1 μM, ATP 400 μM). Both a radioactive and a non-radioactive HPLC assay were used. For the radioactive CaMKII assay, activity was measured as by incorporation of ^{32}P-ATP into a synthetic substrate (syntide-2) at 30°C, as previously described (15). The reaction was stopped with 10mM EGTA. For the non-radioactive assay, phosphorylated and non-phosphorylated peptides were separated with the HPLC system and column described above for HPLC-mass spectrometry except that the acetonitrile gradient was developed as: 0-10%, 0-2 min; 10-22%, 2-26 min; 22-95%, 26-30 min; 95-0%, 30.0-30.1 min. Reactions were stopped by addition of 1 μl 20% trifluoroacetic acid. The fraction of phosphorylated peptide was calculated from the integrated areas of the peaks on the UV chromatogram at 210 nm.

Fluorescent anisotropy measurements

The following peptides from the CaM binding domain of CaMKIIδ were synthesized by Genscript: WT ((K-FITC)LKKFNARRKLKGAILTTMLA), M308-SO ((K-FITC)LKKFNARRKLKGAILTTMet(SO)LA), M308V ((K-FITC)LKKFNARRKLKGAILTTVLA) and M308Q ((K-FITC)LKKFNARRKLKGAILTTQLA). The peptides were dissolved in distilled H20 at a concentration of 1μmol/ml. The peptide concentration in each reaction was 380nM. The reaction buffer included: Hepes 50mM, KCl 100mM, MgCl2 1mM, EGTA 50μM, NTA 5mM (pH7.4). Recombinant CaM protein was generated as described (16). Association of CaM with the different peptides from the CaM-binding site of CaMKII was observed as an increase in fluorescence anisotropy of FITC-peptides measured using a fluorimeter with λ excitation at 496nm and emission at 520nm, using slit widths 3nm (excitation) and 10nm (emission) at 25^{o}C. Anisotropy was measured in a single cuvette containing the peptide at baseline and

after the addition of various concentrations of CaM (for CaM titrations) at constant Ca^{2+} concentration (50μM). In Figure 3C CaM concentration was 1600nM.

Preparation of the CaMKIIδ CaM binding domain R-epimer M308-SO peptide
The chemically synthesized FITC-tagged peptide containing CAMKII residues 290-309 with M308-suldoxide is a mixture of R- and S- epimers. The peptide was incubated with MSRA to reduce the S-epimer M308-SO to M308. The R-epimer M308-SO was purified away from the MSRA and the M308 peptide by reverse phase HPLC. The FITC-tagged peptide (250 μM in 50 mM sodium phosphate with 100 μM diethylenetriaminepentaacetic acid) was incubated overnight at 37ºCwith 10 mM DTT and 50 μg/ml mouse MSRA. The reaction was stopped by addition of $1/200^{th}$ volume of acetic acid. Analytical HPLC-MS showed a decrease in the starting peptide of 50% and an equal increase in the M308 form of the peptide, indicating that the reaction went to completion. Preparative HPLC was then performed on a Vydac 218TP5205 C18 column. The flow rate was 0.2 ml/min, and chromatograms were obtained at 210 nm and 495 nm (FITC). The initial solvent was water/0.05% trifluoroacetic acid. Peptides were eluted by a gradient with acetonitrile/0.05% trifluoroacetic acid. The gradient was 0-15% from 0-3 min, then 15-35% from 3-23 min. Under these conditions, the R-epimer M308-SO peptide eluted first and was separated from the M308 peptide separated by 2 min. Analysis of the collected R-epimer M308-SO fraction by HPLC-MS confirmed that it was free of the M308 peptide.

Computational structural and CaMKII activity modeling

Computational modeling of CaMKII M308, M308-SO, M308V and M308Q binding to CaM
To model the effects of substituting the sidechain of CaMKII M308 with M308-SO (R stereoisomer), V (valine) or Q (glutamine), the crystallographic structure 1CM1.pdb (2 Å resolution; (17)) was chosen as the wild-type conformation of $(Ca^{2+})_4$-CaM bound to the CaM-binding domain of CaMKII (residues 294-311). Initial computational mutagenesis was done with PyMOL (Schrödinger, LLC), using the h-add command to add hydrogens. The PyMOL Mutagenesis Wizard tool introduced a replacement sidechain (M308V or M308Q); the rotamer with the highest likelihood was used as an initial conformer. Oxidized methionine (M308-SO) was created in PyMOL using the Build Fragment tool to add a methyl group and replace the methyl with an oxygen to create the R stereoisomer (M308-SO). The coordinates for these initial models and the original crystallographic structure (1CM1) were energy-minimized with Yasara (version 18.4.24.M.32; (18)) applying the Amber14 force field (TIP3P water model) to a cube (70 Å on a side, periodic boundary conditions), with 0.9% NaCl at 25° C (298 K), pH 7.4. Convergence was defined as an energy change of less than 0.05 kJ/mol/atom per iteration. For each mutation or modification, the energy-minimized structure was used as the initial model for a molecular dynamics (MD) simulation in Yasara (18) using the macro md_run to allow the protein complex to relax. Parameters for the solvent conditions and volume were identical to those of the initial energy minimization. The MD run (elapsed time of ~24 h) sampled an interval of 10 ns with a time-step of 2.5 fs (femtosecond), saving 100 simulation snapshots that included total potential energy,

RMSD (root-mean-square-difference) from the initial model, and atomic coordinates at 100 ps intervals. Movies 1-4 that show the initial model made by PyMOL, the model resulting from energy minimization by Yasara, and 100 snapshots of the MD Trajectories are included as multimedia files. Throughout the MD run, potential energy varied by less than 1%, but local rearrangements near CaMKII sidechain 308 occurred. To represent an average structure, 100 snapshots from the MD run were spatially averaged, and energy minimized to assure adherence to chemically allowed stereochemistry. The models are shown in Figure 3A and Supplemental Figure 1C, highlighting positions of residues E84, I85, A88 and M145 that are within 4.5 Å of M308 in the crystallographic structure 1CM1.pdb. As a positive control, the WT M308 model from Yasara was compared to multiple conformers experimentally reported in 1CM4.pdb (17); the orientation of the M308 sidechain closely matched conformer "D", giving confidence in the computational approach. Contacts of Structural Units (CSU) were derived with CSU software (19) to compare effects of substitutions of V, Q or sulfoxide of M308 on interactions with atoms in sidechains of CaM.

CaMKII activity simulations

A four-state CaMKII model and a four step sequential model for CaM binding were used to describe the process of activation of CaMKII as previously described (20). The model assumed same activity for all three CaMKII active states: $(Ca^{2+})_4$-CaM-bound state , autophosphorylated $(Ca^{2+})_4$CaM-bound state , and autophosphorylated $(Ca^{2+})_4$CaM-dissociated state. The non-active state is CaMKII. The mathematical expression and parameters were taken as previously described (20) for the δ isoform of CaMKII and adjusted to fit the experimental results from Figure 3B in order to compare WT, M308-SO, M308V and M308Q CaMKII activities based on the different binding affinities of their CaM-binding domain to CaM. The model simulations were implemented in MATLAB 2017a (The MathWorks, Natick, MA) and the ordinary differential equations were solved by the ODE solver *ode15s*. The optimization was performed using *fmincon* function in MATLAB optimization toolbox to find the dissociation constants (Table 2). To simulate CaMKII dynamics under normal and CPTV conditions, resting calcium level was set as 2 times higher than normal resting calcium level and the calcium amplitude was set to be the same under normal and CPTV conditions as previously described (21). WT, M308-SO, M308Q and M308V CaMKII were simulated with the adjusted parameter *k asso* (Table 2). Frequency-dependent activation of CaMKII was simulated from 0.5Hz to 6Hz in the presence of ATP and protein phosphatase 1 (PP1), and the calcium pulse period was kept at constant at 160ms or varied from 80ms to 1000ms to test the calcium activation relationship (22).

Intracellular Ca^{2+} simulations

Effects of the M308V CaMKII on intracellular Ca^{2+} cycling were simulated using a well-validated mathematical model of the human cardiac action potential with modifications to incorporate the CaMKII signaling pathway (23, 24). The rate constant of Ca^{2+}/CaM binding to CaMKII was reduced from its control value in M308V to fit experimental measurements (Supplemental Figure 4A). The control (WT) and M308V cell models were then paced at a basic cycle length of 1000ms to steady state under conditions of elevated CaMKII activity (amount of Ca^{2+}/CaM bound to CaMKII increased by factor of

5. To determine relative importance of specific CaMKII targets in observed differences, a subset of simulations was run with effects of CaMKII on phospholamban, ryanodine receptor, or late Na^+ current eliminated.

Human iPSC studies

Differentiation to iPSC-derived cardiomyocytes

Human iPSCs were seeded onto Matrigel-coated dishes at normal passage density. -- IPSC differentiation to iPSC-CMs followed the following timeline: on day 3 of iPSC culture, mTeSR1 medium was removed, cells were rinsed once with PBS (without Ca^{2+} or Mg^{2+}), and cultured in Differentiation Medium (RPMI medium (11875093, Thermo Fisher Scientific) with B27 without insulin (A1895601, Thermo Fisher Scientific)) containing 5-8 μM CHIR99021 (72054, STEMCELL Technologies). After 24 hours, medium was changed to differentiation medium without CHIR99021. At differentiation day 3, cells were cultured in differentiation medium containing 5 μM IWR-1 (3532, Tocris). After 48 hours, cells were cultured in differentiation medium without IWR until day 15, with media changes every 2-3 days. At day 15, the cells were cultured in Selection Medium (Non-Glucose DMEM (11966025, Thermo Fisher Scientific) with 5 mM Lactate (# L7022, Sigma Aldrich) for 5 days to enrich for iPSC-CMs. To create the seeding solution for the opto-MTF, iPSC-CMs were isolated by incubating in collagenase 1 (Sigma C-0130, 100mg collagenase 1 in 50 ml PBS/20% FBS) for 1 hour, followed by a 0.25% Trypsin incubation at 37°C for 5-10 mins. 50% FBS in DMEM with 50 μg/ml DNase I (# 260913, EMD Millipore) was used to stop trypsinization. The iPSC-CMs were suspended in Culture Medium (RPMI:Non-Glucose DMEM 1:1, plus 1x B27 without insulin and 5 mM Lactate) containing 10% FBS and 10 μM Y27632.

Ca^{2+} imaging of iPSC-derived cardiomyocytes

IPSC-CMs were seeded on 0.1% gelatin and Geltrex-coated coverslips. After 24 hours, cells were transduced with adenovirus that expresses the GCaMP6f-Junctin nanosensor (6f-J) (25). After 48 hours, the coverslips were placed in an imaging chamber (IonOptix) and a temperature of 36-37°C was maintained by using a mini-peristaltic pump to circulate extracellular buffer through an in-line heater regulated by a closed-loop controller. The samples were imaged on an Olympus FV3000R using line scan mode (2 msec/line, 15000 lines per recording). The scan line was positioned within individual iPSC-CMs through the longest dimension to maximize recording cell area. Extracellular buffer containing (in mM) NaCl 140, KCl 4, $MgCl_2$ 2, $CaCl_2$ 1.2, HEPES 10, Glucose 15, and sodium pyruvate 2, with pH of 7.4, was supplemented with 1 μM isoproterenol (ISO). Isoproterenol was circulated through the imaging chamber for at least 5 minutes prior to imaging.

Quantification of protein expression for iPSC-derived cardiomyocytes

Western blots for all four iPSC lines were collected using the Protein Simple Wes™ system. After lactate selection, eight cell populations from each line were individually

collected, four of which were treated with 1uM isoproterenol and incubated at 37°C for 5 min. After prompt washing with PBS, lysate was extracted using MTOR lysis buffer solution (120mM NaCl, 40mM HEPES, 1mM EDTA, 40mM NaI, 10mM β-glycerophosphate, 0.3% CHAPS at pH 7.5) with 1% Triton-X-100 and Halt™ Protease & Phosphatase Inhibitor. Lysate was normalized to 0.25mg/ml and loaded at a final concentration of 0.2mg/ml after addition of Wes kit reagents. Primary antibodies, CaMKII antibody (Rb mAb, Abcam, ab134041), Phospho-CaMKII (Rb mAb, Cell Signaling Technology #12716), GAPDH (Rb pAb, Invitrogen #PA1-16777), were optimized and loaded at dilutions of 1:100, 1:50, 1:400 and 1:200, respectively. Kit-provided anti-Rb secondary antibody was used for all samples. Run per manufacturer's recommendations. Band areas quantified using Protein Simple's *Compass for SW* system.

Flow-cytometry of iPSC-derived cardiomycytes

IPSC-CMs were isolated using the STEMdiff CM dissociation kit (STEM Cell technologies) and washed once with PBS. Cells were then fixed with BD Cyto Fix/Perm buffer (BD Biosciences) for 20 minutes at room temperature. Cells were washed twice with Perm/Wash buffer (BD Biosciences) and then stained for cardiac Troponin-T (cTnT) at 1:50 with a FITC-conjugated antibody (Miltenyi Biotechnologies) and then incubated at 4 degrees in the dark for one hour. Cells were analyzed using a BD LSRFortessa (BD Biosciences) cell analyzer. An isotype IgG stained sample served as a control.

1. Gupta A, Akki A, Wang Y, Leppo MK, Chacko VP, Foster DB, et al. Creatine kinase-mediated improvement of function in failing mouse hearts provides causal evidence the failing heart is energy starved. *The Journal of clinical investigation.* 2012;122(1):291-302.
2. Wu Y, Gao Z, Chen B, Koval OM, Singh MV, Guan X, et al. Calmodulin kinase II is required for fight or flight sinoatrial node physiology. *Proc Natl Acad Sci U S A.* 2009;106(14):5972-7.
3. Wu Y, Shintani A, Grueter C, Zhang R, Hou Y, Yang J, et al. Suppression of dynamic Ca(2+) transient responses to pacing in ventricular myocytes from mice with genetic calmodulin kinase II inhibition. *Journal of molecular and cellular cardiology.* 2006;40(2):213-23.
4. Rasmussen TP, Wu Y, Joiner ML, Koval OM, Wilson NR, Luczak ED, et al. Inhibition of MCU forces extramitochondrial adaptations governing physiological and pathological stress responses in heart. *Proc Natl Acad Sci U S A.* 2015;112(29):9129-34.
5. Sokolove PG, and Bushell WN. The chi square periodogram: its utility for analysis of circadian rhythms. *Journal of theoretical biology.* 1978;72(1):131-60.
6. Vogler G, and Ocorr K. Visualizing the beating heart in Drosophila. *Journal of visualized experiments : JoVE.* 2009(31).
7. Cammarato A, Ocorr S, and Ocorr K. Enhanced assessment of contractile dynamics in Drosophila hearts. *BioTechniques.* 2015;58(2):77-80.

8. Fink M, Callol-Massot C, Chu A, Ruiz-Lozano P, Izpisua Belmonte JC, Giles W, et al. A new method for detection and quantification of heartbeat parameters in Drosophila, zebrafish, and embryonic mouse hearts. *BioTechniques.* 2009;46(2):101-13.
9. Blice-Baum AC, Zambon AC, Kaushik G, Viswanathan MC, Engler AJ, Bodmer R, et al. Modest overexpression of FOXO maintains cardiac proteostasis and ameliorates age-associated functional decline. *Aging cell.* 2017;16(1):93-103.
10. Viswanathan MC, Schmidt W, Rynkiewicz MJ, Agarwal K, Gao J, Katz J, et al. Distortion of the Actin A-Triad Results in Contractile Disinhibition and Cardiomyopathy. *Cell reports.* 2017;20(11):2612-25.
11. Lee BC, Peterfi Z, Hoffmann FW, Moore RE, Kaya A, Avanesov A, et al. MsrB1 and MICALs regulate actin assembly and macrophage function via reversible stereoselective methionine oxidation. *Molecular cell.* 2013;51(3):397-404.
12. Hung RJ, Pak CW, and Terman JR. Direct redox regulation of F-actin assembly and disassembly by Mical. *Science (New York, NY).* 2011;334(6063):1710-3.
13. Apffel A, Fischer S, Goldberg G, Goodley PC, and Kuhlmann FE. Enhanced sensitivity for peptide mapping with electrospray liquid chromatography-mass spectrometry in the presence of signal suppression due to trifluoroacetic acid-containing mobile phases. *JChromatogrA.* 1995;712(1):177-90.
14. Levine RL. Fixation of nitrogen in an electrospray mass spectrometer. *Rapid Commun Mass Spectrom.* 2006;20(12):1828-30.
15. Erickson JR, Joiner ML, Guan X, Kutschke W, Yang J, Oddis CV, et al. A dynamic pathway for calcium-independent activation of CaMKII by methionine oxidation. *Cell.* 2008;133(3):462-74.
16. Evans TI, and Shea MA. Energetics of calmodulin domain interactions with the calmodulin binding domain of CaMKII. *Proteins.* 2009;76(1):47-61.
17. Wall ME, Clarage JB, and Phillips GN. Motions of calmodulin characterized using both Bragg and diffuse X-ray scattering. *Structure (London, England : 1993).* 1997;5(12):1599-612.
18. Krieger E, and Vriend G. New ways to boost molecular dynamics simulations. *Journal of computational chemistry.* 2015;36(13):996-1007.
19. Sobolev V, Sorokine A, Prilusky J, Abola EE, and Edelman M. Automated analysis of interatomic contacts in proteins. *Bioinformatics (Oxford, England).* 1999;15(4):327-32.
20. Chiba H, Schneider NS, Matsuoka S, and Noma A. A simulation study on the activation of cardiac CaMKII delta-isoform and its regulation by phosphatases. *Biophysical journal.* 2008;95(5):2139-49.
21. Kujala K, Paavola J, Lahti A, Larsson K, Pekkanen-Mattila M, Viitasalo M, et al. Cell model of catecholaminergic polymorphic ventricular tachycardia reveals early and delayed afterdepolarizations. *PloS one.* 2012;7(9):e44660.
22. De Koninck P, and Schulman H. Sensitivity of CaM kinase II to the frequency of Ca2+ oscillations. *Science (New York, NY).* 1998;279(5348):227-30.
23. Onal B, Gratz D, and Hund TJ. Ca(2+)/calmodulin-dependent kinase II-dependent regulation of atrial myocyte late Na(+) current, Ca(2+) cycling, and excitability: a mathematical modeling study. *American journal of physiology Heart and circulatory physiology.* 2017;313(6):H1227-h39.

24. Grandi E, Pandit SV, Voigt N, Workman AJ, Dobrev D, Jalife J, et al. Human atrial action potential and Ca2+ model: sinus rhythm and chronic atrial fibrillation. *Circ Res.* 2011;109(9):1055-66.
25. Shang W, Lu F, Sun T, Xu J, Li LL, Wang Y, et al. Imaging Ca2+ nanosparks in heart with a new targeted biosensor. *Circ Res.* 2014;114(3):412-20.

Supplemental Figure Legends

Figure S1. CaM binding domain M308 is highly conserved across species and oxidized by MICAL1. Structural modeling of interactions **between reduced and oxidized M308 with CaM. (A)** The CaM-binding domain, including M308, of all CaMKII isoforms is conserved among *Mus musculus*, *Homo sapiens* and *Drosophila melanogaster*. **(B)** M308-SO is markedly increased after incubation of CaMKII with MICAL1 as detected by mass spectrometry. **(C)** Models of interface between $(Ca^{2+})_4$-CaM residues E84, I85, A88 and M145 and CaMKII M308 or M308-SO shown from two viewpoints (rotated by 90˚ about the vertical Y-axis). CaM sidechains E84, I85, A88, and M145 are red sticks, with E84 carboxyl oxygens (OE1, OE2) highlighted in pink, and M145 sulfur shown as a yellow-orange sphere (35% van der Waals radius). CaMKII WT M308 (black) and mutant M308-SO (green) heteroatoms are spheres (100% van der Waals radius) with the sulfur highlighted as yellow-orange, and hydrogen atoms colored white. The oxygen of M308-SO is shown in forest green. Models were aligned based on the backbone of CaMKII residues 294-311 (gray cylinder). Models were based on averages of Yasara Molecular Dynamics trajectories for computational mutation of M308 (initial WT model was crystallographic structure 1cm1.pdb) to Met-SO (see *Supplementary Methods*).

Figure S2. *MICAL1*$^{-/-}$ mouse hearts at baseline and after pathological cardiac stress. Structural modeling of MICAL1 and CaMKII interaction. F-actin in *MICAL1*$^{-/-}$ and *MICAL1*^{R116H} mice. (A and B) Western blots showing no difference between WT and MICAL1$^{-/-}$ heart lysates in RyR2 **(A)** or SERCA **(B)** at baseline (n=5 in each group; right panels in each figure show quantification data). (**C)** Isolated adult cardiomyocytes from WT and MICAL1$^{-/-}$ mouse hearts show no difference at baseline in cytoplasmic Ca^{2+} decay slope, diastolic Ca^{2+} level, Ca^{2+} peak amplitude, or SR Ca^{2+} content (WT n=3 mice, n=16 cells *(Ca^{2+} decay slope, diastolic Ca^{2+} level, Ca^{2+} peak amplitude),n= 47 cells (SR Ca2+ content); MICAL1$^{-/-}$* n=3 mice, n=8-22 cells *(Ca^{2+} decay slope, diastolic Ca^{2+} level, Ca^{2+} peak amplitude) n= 40 cells (SR Ca2+ content))* **(D)** Serial echocardiograms in WT and MICAL1$^{-/-}$ mice at baseline, 3 days, 7 days and 14 days post-TAC show no difference in left ventricular function between the two groups. (WT mice n=6, MICAL1$^{-/-}$ mice n=8) **(E)** Implanted telemeters in *MICAL1*$^{-/-}$ mice detect significant arrhythmias including severe bradycardia and agonal rhythm preceding their death after TAC **(F)** CaMKII (PDB Id: 3SO4) exhibits significant complementarity with the α-helix-rich side of the reduced monooxygenase domain of MICAL1 (PDB Id: 2C4C) (Siebold et al., 2005). CaMKII can be manually placed with M308 reaching the catalytic site widened by the FAD reduction. The remaining unfavorable interactions can be accommodated with small perturbations of loops adjacent to the proteins' contacts. **(G)** The reduction of the MICAL1-FAD by NADPH is coupled with a conformational change in MICAL1 that opens a tunnel to bind and catalyze substrate oxidation. The adenosine pocket anchors the FAD 'tail' allowing its isoalloxazine 'head' to bend and swing into the catalytic site during reduction. R116 forms part of the FAD adenosine binding pocket

and forms a hydrogen-bond with the adenosine ribose. The R116H mutation eliminates a polar interaction and a positive charge that stabilizes the FAD phosphates. The smaller histidine residue also widens the pocket decreasing its complementarity with the adenosine of FAD. The hydroxyperoxyl-FAD was modeled from the reduced FAD. The program MOE was used for the modeling and figures. **(H)** Successful generation of *MICAL1*^{R116H} mice using sanger sequencing. **(I)** Representative images of F-actin assessment using phalloidin-Alexa568 (red) and DAPI (blue) in WT, *MICAL1*$^{-/-}$, and *MICAL1*^{R116H} left ventricular free wall whole mount samples (n= 4 hearts per condition with 10 fields of view imaged and assessed across the entire left ventricular free wall). Scale bar represents 50 μm. Statistical analysis in **(A-D)** performed by two-tailed Student's t-test.

Figure S3. R-stereospecific M308-sulfoxide binding to CaM and computational modeling of CaMKII activity with oxidized or mutated M308. (A) The racemic mixture of the M308-SO peptide was treated with MSRA to reduce the S-stereospecific M308-SO peptide (top panel; before purification) and then the R-stereospecific M308-SO containing peptide was purified (bottom panel; after purification). **(B)** The R-stereospecific M308-SO (Met R-SO) peptide showed decreased binding to Ca^{2+}/CaM compared to the peptide with reduced M308 (WT) as assessed by fluorescence anisotropy. Data represented as the mean of n=3 replicates +/- SEM. ($p<0.001$(***)) by two-tailed Student's t-test. **(C)** Computational modeling of CaMKII activity responses to Ca^{2+} stimulation frequencies (0.1 to 5 Hz) using increasing pulse durations (80, 200, 500, and 1000 ms) at various calmodulin (CaM) concentrations (indicated in red above each panel). The Ca^{2+} concentration was held constant for each pulse (basal Ca^{2+} at $0.5\mu M$, peak Ca^{2+} at $4\mu M$). Note that M308-SO and M308V curves at various pulsing periods are superimposed. **(D)** Computational modeling of CaMKII activity responses to Ca^{2+} stimulation frequencies (0.1 to 5 Hz) using increasing pulse durations (80, 200, 500, and 1000 ms) over a range of Ca^{2+} concentrations (peak concentration of Ca^{2+} pulses indicated in red above each panel). The calmodulin (CaM) concentration was held constant at 10 μM. Note that M308-SO and M308V curves at various pulsing periods are superimposed.

Figure S4: Ca^{2+} dynamics simulations in WT and M308V cardiac myocytes and CaMKII activation in *CaMKII*δ^{M308V} mice. (A) Simulated (sim) WT and M308V CaMKII activity as a function of calmodulin concentration and binding compared to experimental (exp) measurements (experimental measurements obtained from data used in Fig. 3b). The rate constant for Ca^{2+}/CaM binding to CaMKII was fit to minimize mean squared error between simulation and experiment. **(B)** Simulated Ca^{2+} transients during steady-state pacing of the action potential model with WT or M308V CaMKII under control conditions (left panel) or following elimination of CaMKII-dependent effects on phospholamban (PLB) (right panel). The M308V model shows a noticeable slowing in

decay of the Ca^{2+} transient compared to WT, which is normalized by eliminating effects of CaMKII on PLB. **(C)** Sanger sequencing showing successful generation of *CaMKIIδ*^{M308V} mice. **(D)** Western blot of autophosphorylated T-287 (p-CaMKII) and total-CaMKII (t-CaMKII) in WT and *CaMKIIδ*^{M308V} mice 5 minutes after intraperitoneal isoproterenol injection (0.4mg/Kg/mouse) (n=4 mice in both groups). Quantification of the western blot data (top panel) is shown (bottom panel). ($p<0.01$ (**)) by two-tailed Student's t-test.

Figure S5. Cardiac function in *CaMKII*^{M308V} *Drosophila melanogaster*. (A) Successful generation of *CaMKII*^{M308V} *Drosophila melanogaster* using CRISPR was confirmed with Sanger sequencing. **(B-D),** *CaMKII*^{M308V} fly heart tubes exhibit **(B)** smaller diastolic diameters, **(C)** smaller systolic diameters and **(D)** shorter diastolic intervals compared to WT flies. **(E)** Diameter of *CaMKII*^{M308V} heart tubes after Ca^{2+} chelation with EGTA and EGTA-AM. ($p<0.001$ (***)) by two-tailed Student's t-test **(B-D)** and two-tailed paired t-test **(E)**.

Figure S6. Differentiation of hiPSCs to cardiomyocytes. Flow cytometry showing differentiation of hiPSCs (WT, WT-*CaMKIIδ*^{M308V}, CPVT, CPVT-*CaMKIIδ*^{M308V}) to cardiomyocytes as measured by c-TnT staining.

Figure S1

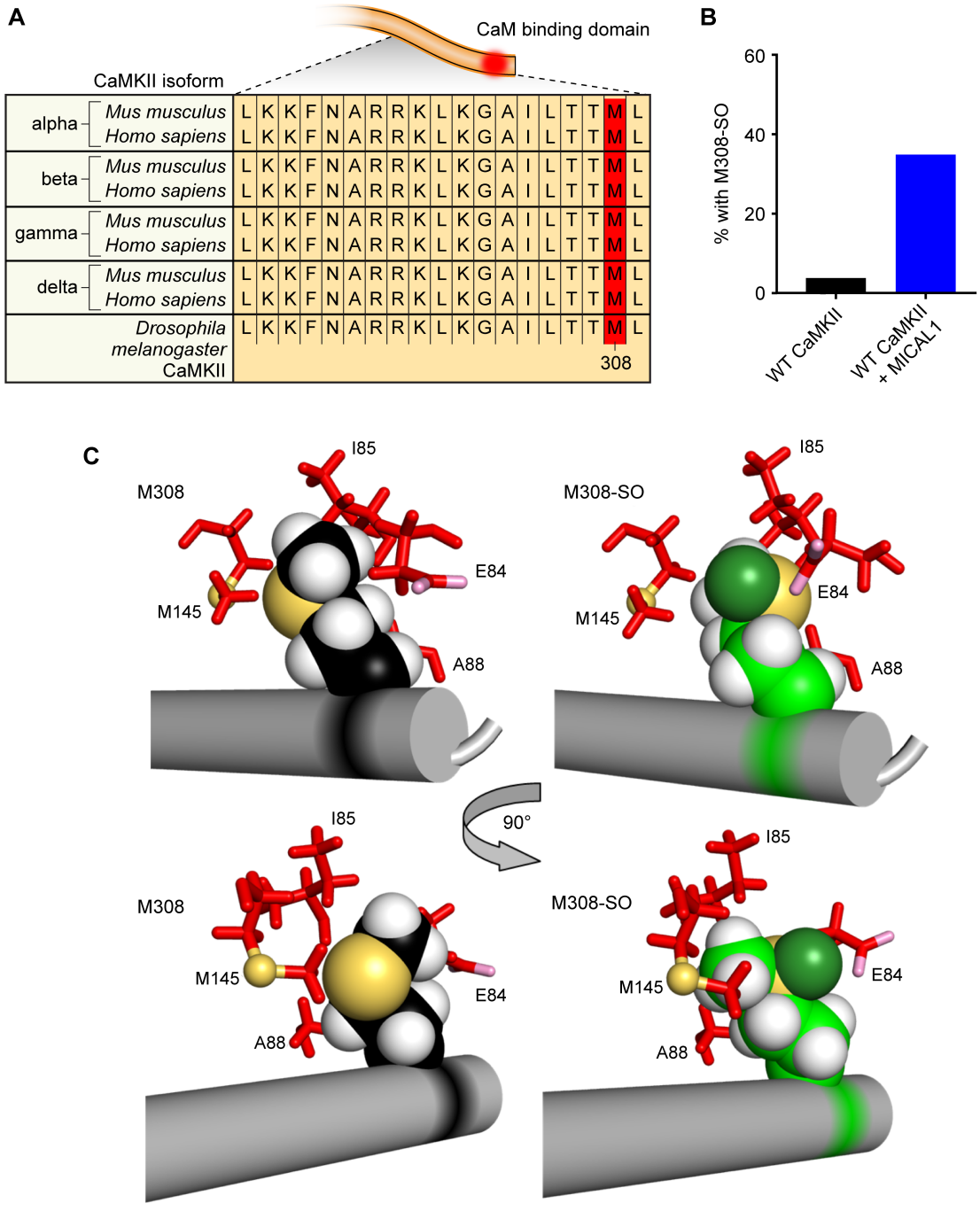
A
CaM binding domain
CaMKII isoform
alpha
Mus musculus L K K F N A R R K L K G A I L T T M L
Homo sapiens L K K F N A R R K L K G A I L T T M L
beta
Mus musculus L K K F N A R R K L K G A I L T T M L
Homo sapiens L K K F N A R R K L K G A I L T T M L
gamma
Mus musculus L K K F N A R R K L K G A I L T T M L
Homo sapiens L K K F N A R R K L K G A I L T T M L
delta
Mus musculus L K K F N A R R K L K G A I L T T M L
Homo sapiens L K K F N A R R K L K G A I L T T M L
Drosophila melanogaster CaMKII L K K F N A R R K L K G A I L T T M L
308
B
% with M308-SO
60
40
20
0
WT CaMKII
WT CaMKII + MICAL1
C
I85
M308
E84
M145
A88
M308-SO
90°

Figure S2

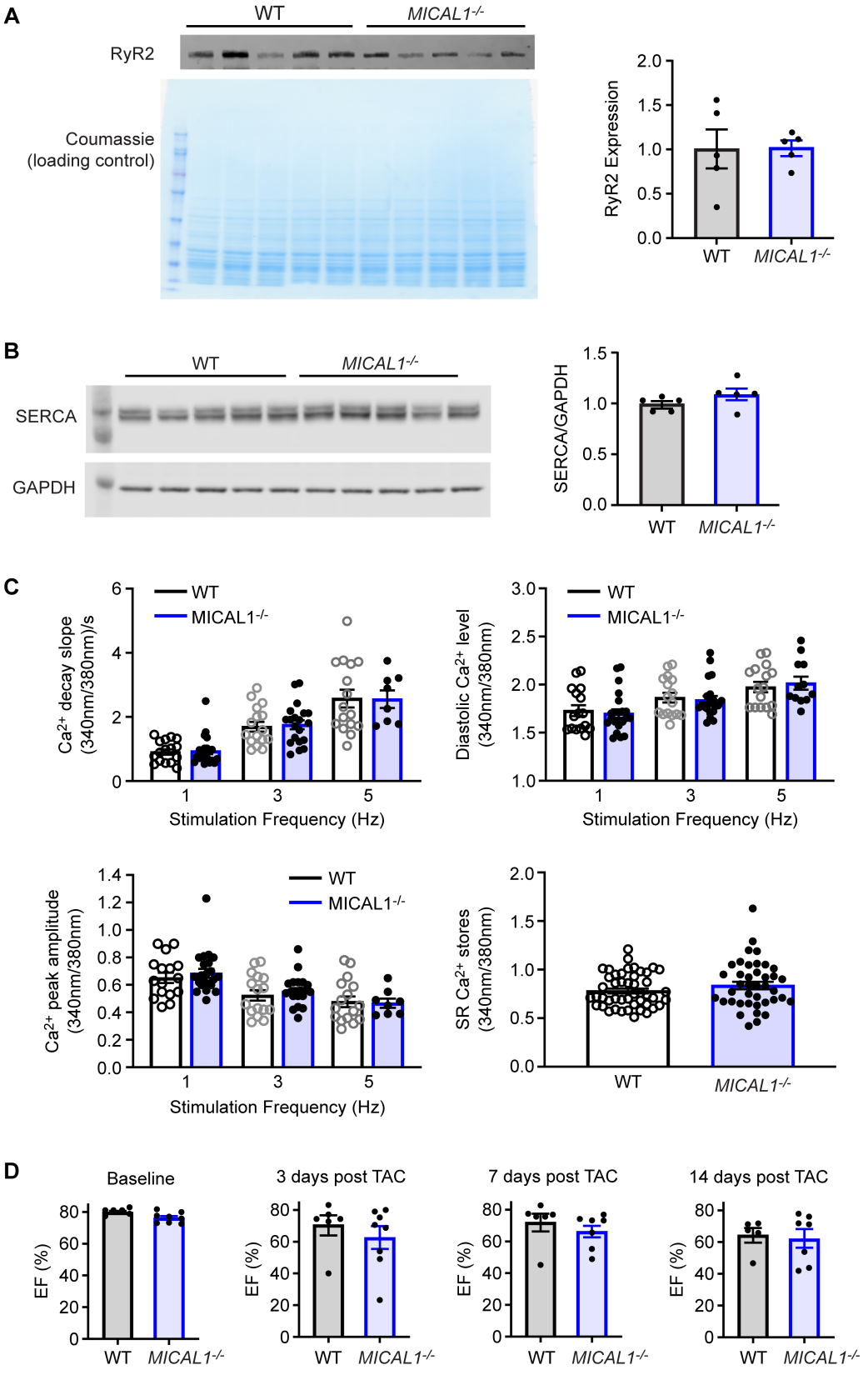
A
WT
MICAL1-/-
RyR2
Coumassie
(loading control)
RyR2 Expression
2.0
1.5
1.0
0.5
0.0
WT
MICAL1-/-
B
WT
MICAL1-/-
SERCA
GAPDH
SERCA/GAPDH
1.5
1.0
0.5
0.0
WT
MICAL1-/-
C
WT
MICAL1-/-
Ca2+ decay slope (340nm/380nm)/s
6
4
2
0
1
3
5
Stimulation Frequency (Hz)
Diastolic Ca2+ level (340nm/380nm)
3.0
2.5
2.0
1.5
1.0
Ca2+ peak amplitude (340nm/380nm)
1.4
1.2
1.0
0.8
0.6
0.4
0.2
0.0
SR Ca2+ stores (340nm/380nm)
2.0
1.5
1.0
0.5
0.0
D
Baseline
3 days post TAC
7 days post TAC
14 days post TAC
EF (%)
80
60
40
20
0
WT
MICAL1-/-

Figure S2

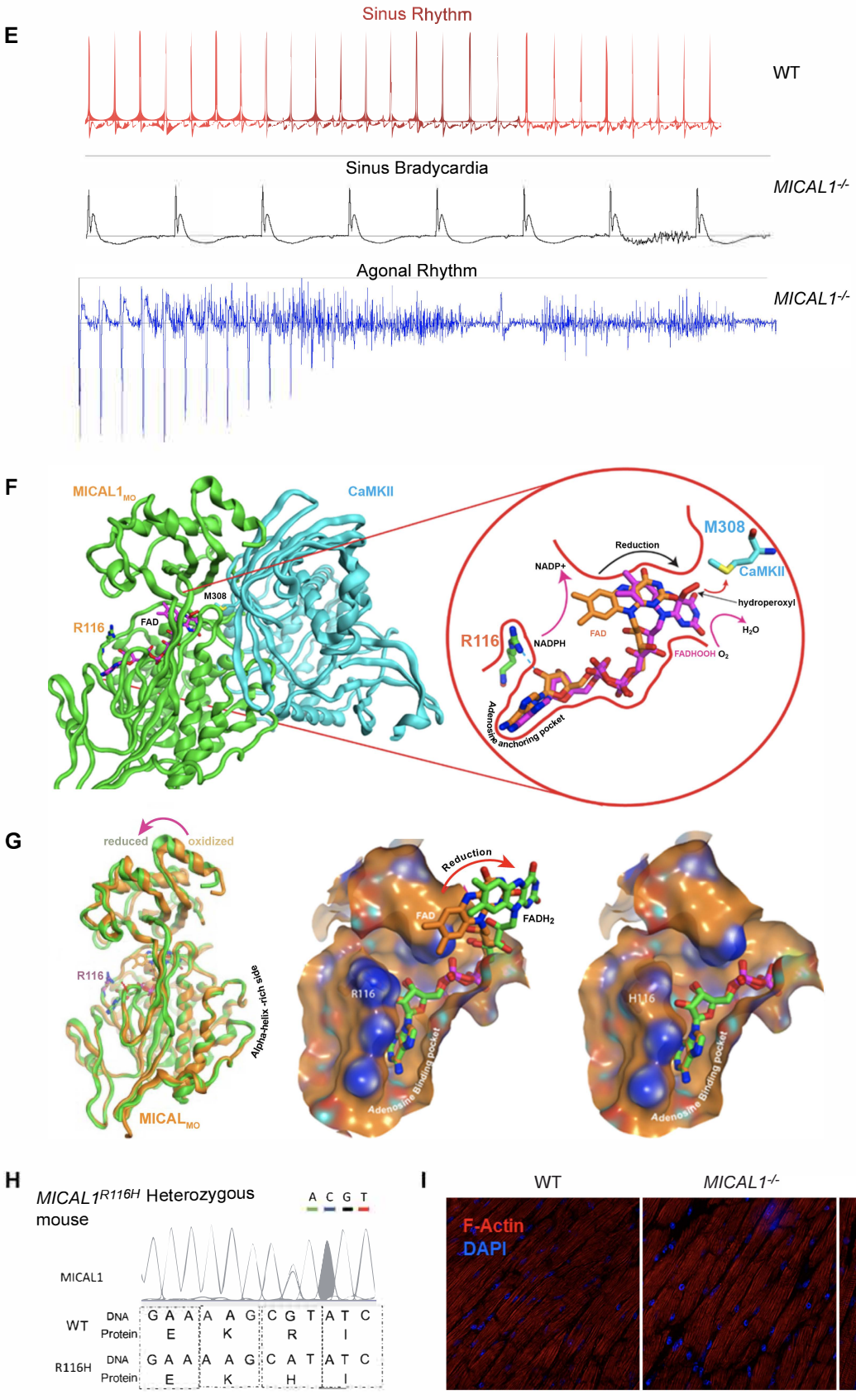
E
Sinus Rhythm
WT
Sinus Bradycardia
MICAL1-/-
Agonal Rhythm
MICAL1-/-
F
MICAL1MO
CaMKII
M308
R116
FAD
Reduction
NADP+
NADPH
hydroperoxyl
H2O
FADHOOH O2
Adenosine anchoring pocket
G
reduced
oxidized
R116
Alpha-helix -rich side
MICALMO
Reduction
FAD
FADH2
Adenosine Binding pocket
H
MICAL1R116H Heterozygous mouse
A C G T
MICAL1
WT
DNA G A A A A G C G T A T C
Protein E K R I
R116H
DNA G A A A A G C A T A T C
Protein E K H I
I
WT
MICAL1-/-
MICAL1R116H
F-Actin
DAPI
50 μm

Figure S3

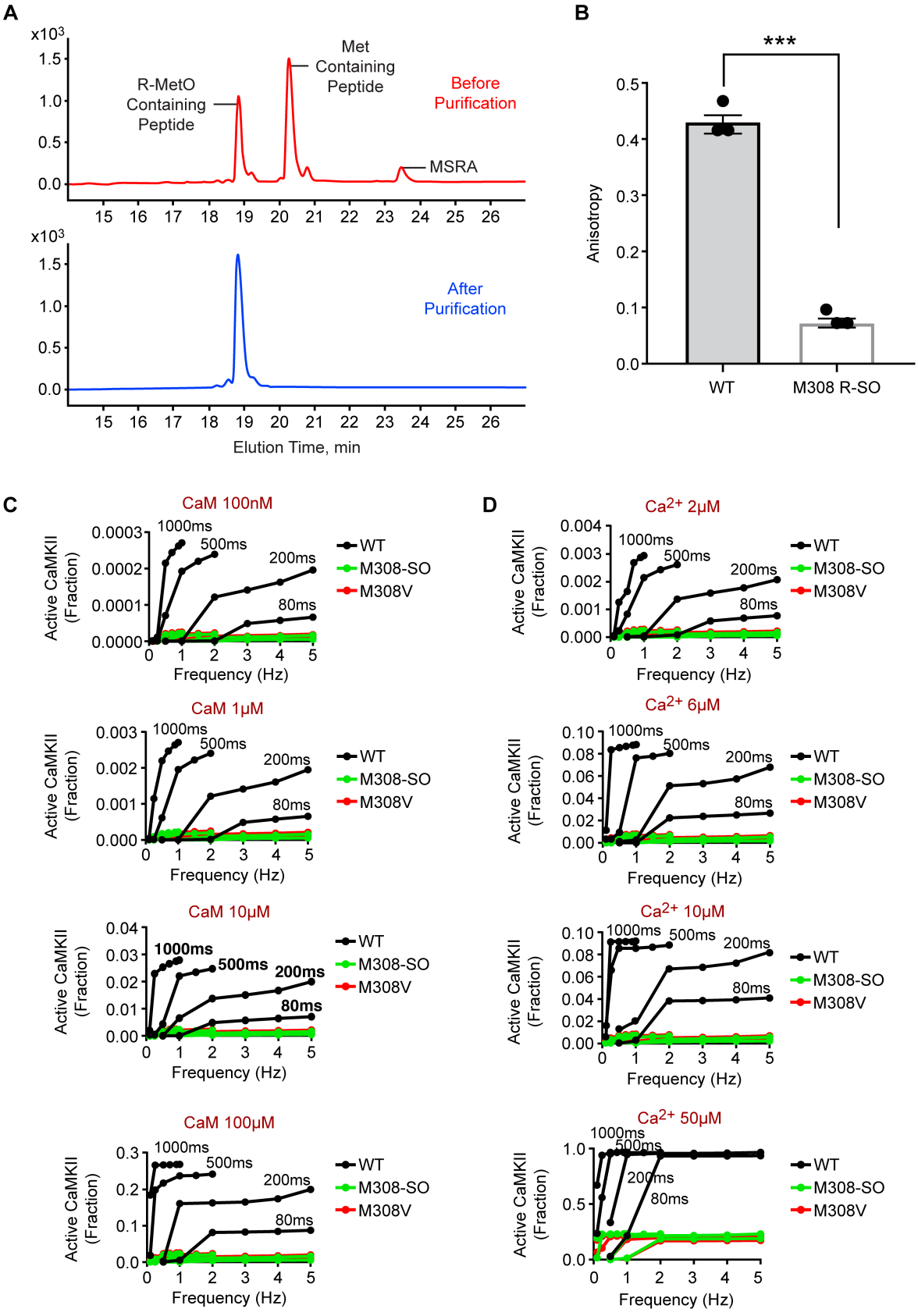
A
x10^3
1.5
1.0
0.5
0.0
R-MetO Containing Peptide
Met Containing Peptide
Before Purification
MSRA
15 16 17 18 19 20 21 22 23 24 25 26
After Purification
Elution Time, min
B
***
Anisotropy
0.5
0.4
0.3
0.2
0.1
0.0
WT
M308 R-SO
C
CaM 100nM
CaM 1μM
CaM 10μM
CaM 100μM
Active CaMKII (Fraction)
Frequency (Hz)
1000ms
500ms
200ms
80ms
WT
M308-SO
M308V
D
Ca2+ 2μM
Ca2+ 6μM
Ca2+ 10μM
Ca2+ 50μM

Figure S4

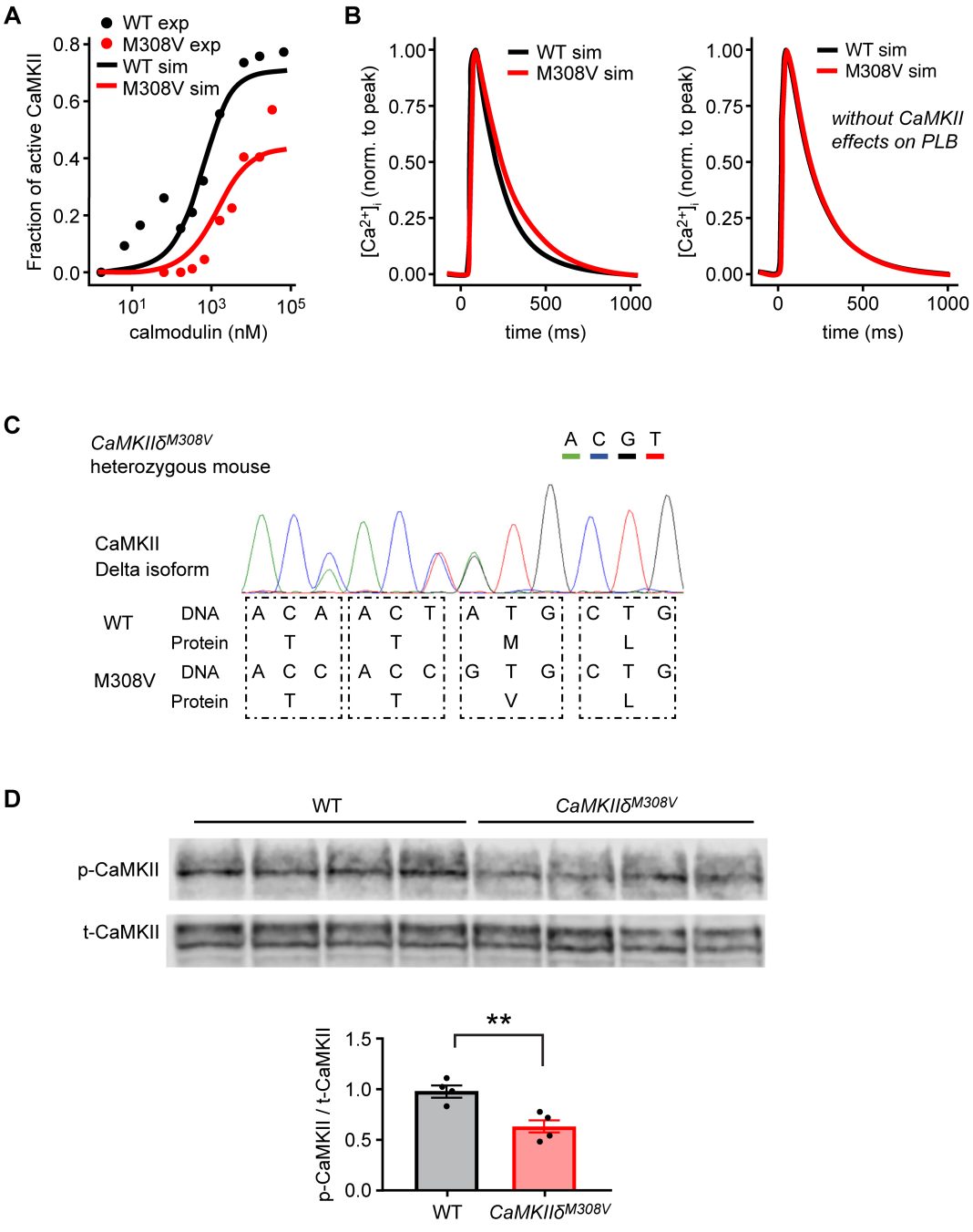
A
WT exp
M308V exp
WT sim
M308V sim
Fraction of active CaMKII
0.8
0.6
0.4
0.2
0.0
10¹
10³
10⁵
calmodulin (nM)
B
WT sim
M308V sim
[Ca2+]i (norm. to peak)
1.00
0.75
0.50
0.25
0.00
0
500
1000
time (ms)
WT sim
M308V sim
without CaMKII
effects on PLB
[Ca2+]i (norm. to peak)
1.00
0.75
0.50
0.25
0.00
0
500
1000
time (ms)
C
CaMKIIδM308V
heterozygous mouse
A C G T
CaMKII
Delta isoform
WT
DNA
A C A A C T A T G C T G
Protein
T T M L
M308V
DNA
A C C A C C G T G C T G
Protein
T T V L
D
WT
CaMKIIδM308V
p-CaMKII
t-CaMKII
**
p-CaMKII / t-CaMKII
1.5
1.0
0.5
0.0
WT
CaMKIIδM308V

Figure S5

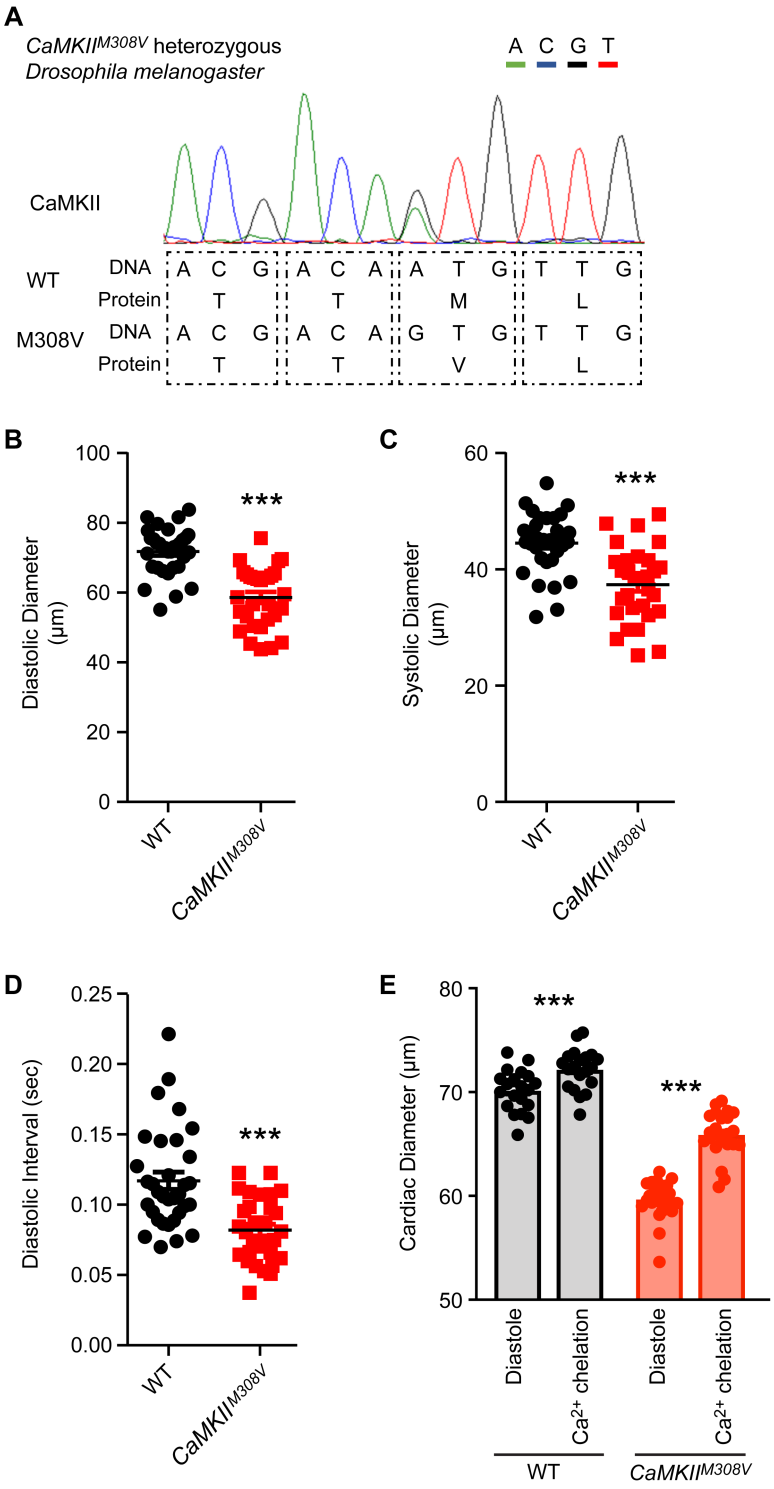
A
CaMKII^M308V heterozygous
Drosophila melanogaster
A C G T
CaMKII
WT
DNA A C G A C A A T G T T G
Protein T T M L
M308V
DNA A C G A C A G T G T T G
Protein T T V L
B
Diastolic Diameter (μm)
100
80
60
40
20
0
***
WT
CaMKII^M308V
C
Systolic Diameter (μm)
60
40
20
0
***
WT
CaMKII^M308V
D
Diastolic Interval (sec)
0.25
0.20
0.15
0.10
0.05
0.00
***
WT
CaMKII^M308V
E
Cardiac Diameter (μm)
80
70
60
50
***
***
Diastole
Ca2+ chelation
Diastole
Ca2+ chelation
WT
CaMKII^M308V

Figure S6

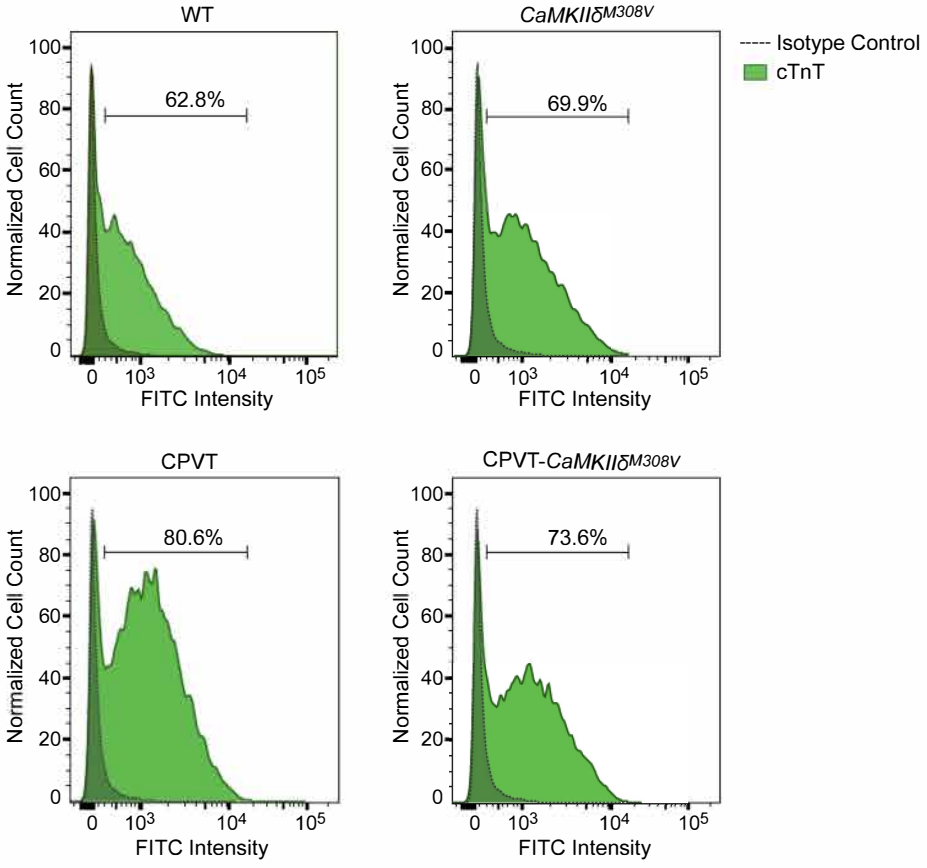
WT
CaMKIIδM308V
CPVT
CPVT-CaMKIIδM308V
62.8%
69.9%
80.6%
73.6%
Normalized Cell Count
FITC Intensity
----- Isotype Control
cTnT

CaMKII activity simulations

Parameter	Value (WT)	Value (mutant)	Description
k_1	2.5 Mm^{-1} ms^{-1}		rate constant (Ca^{2+} binds to CaM)
k_{-1}, k_{-2}	0.05 ms^{-1}		rate constants
k_2	88.25 Mm^{-1} ms^{-1}		rate constant (Ca^{2+} binds to CaM(Ca^{2+}))
k_3	12.5 mM^{-1} ms^{-1}		rate constant(Ca^{2+} binds to CaM(Ca^{2+})$_2$)
k_{-3}, k_{-4}	1.25 ms^{-1}		rate constants
k_4	250 mM^{-1} ms^{-1}		rate constant (Ca2+ binds to CaM(Ca^{2+})$_3$)
k_asso	0.131 mM^{-1} ms^{-1}	0.018 mM^{-1} ms^{-1} (M308-SO) 0.0098 mM^{-1} ms^{-1} (M308V) 0.0038 mM^{-1} ms^{-1} (M308Q)	association rate constant(CaM(Ca^{2+})$_4$ associates to CaMKII)
k_disso	0.7 × 10^{-4} ms^{-1}		dissociation rate constant (CaM(Ca^{2+})$_4$ dissociates from CaMKII_ CaM(Ca^{2+})$_4$)
k_dissoCa2+	0.95 × 10^{-3} ms^{-1}		dissociation rate constant (Ca^{2+} dissociates from CaMKII_ CaM(Ca^{2+})$_4$)
k_disso2	0.7 × 10^{-7} ms^{-1}		dissociation rate constant (CaM(Ca^{2+})$_4$ dissociates from CaMKII_ CaM(Ca^{2+})$_4$)
k_dissoCa2+	0.95 × 10^{-6} ms^{-1}		dissociation rate constant (Ca^{2+} dissociates from CaMKII_ CaM(Ca^{2+})$_4$)
kmCaM	3.0 × 10^{-5} mM		K_d value for the dissociation of Ca^{2+} from CaMKII_ CaM(Ca^{2+})$_4$
kcat	1.8 × 10^{-4} ms_1(30°C) 5.4 × 10^{-3} ms_1(37°C)		rate constant (phosphorylation)
KmATP	19.1 × 10^{-3} mM		Michaelis constant for the CaMKII-ATP complex
kcat_PP1	1.72 × 10^{-3} ms^{-1}		rate constant (dephosphorylation by PP1)
Km_PP1	11.0 × 10^{-3} mM		Michaelis constant for the PP1-CaMKII complex

Table 2. List of parameters used in CaMKII activity simulations

Figure 2A

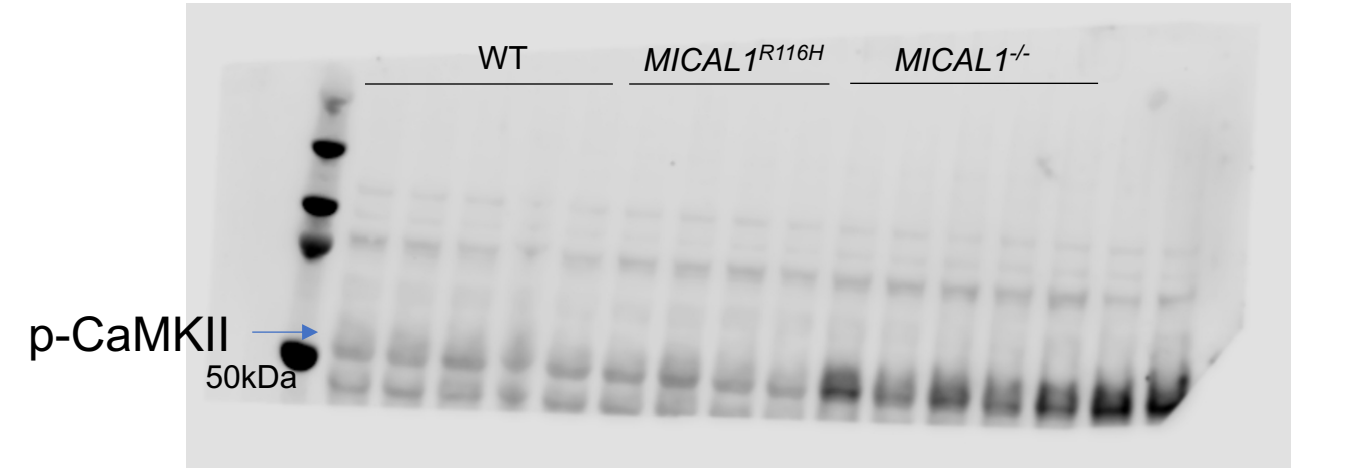
WT
MICAL1R116H
MICAL1-/-
p-CaMKII
50kDa

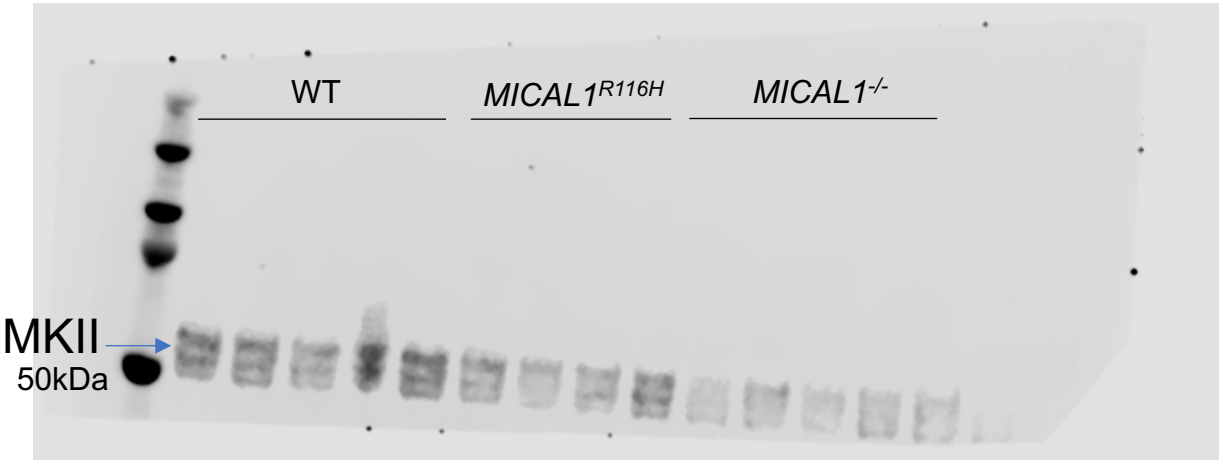
WT
MICAL1R116H
MICAL1-/-
t-CaMKII
50kDa

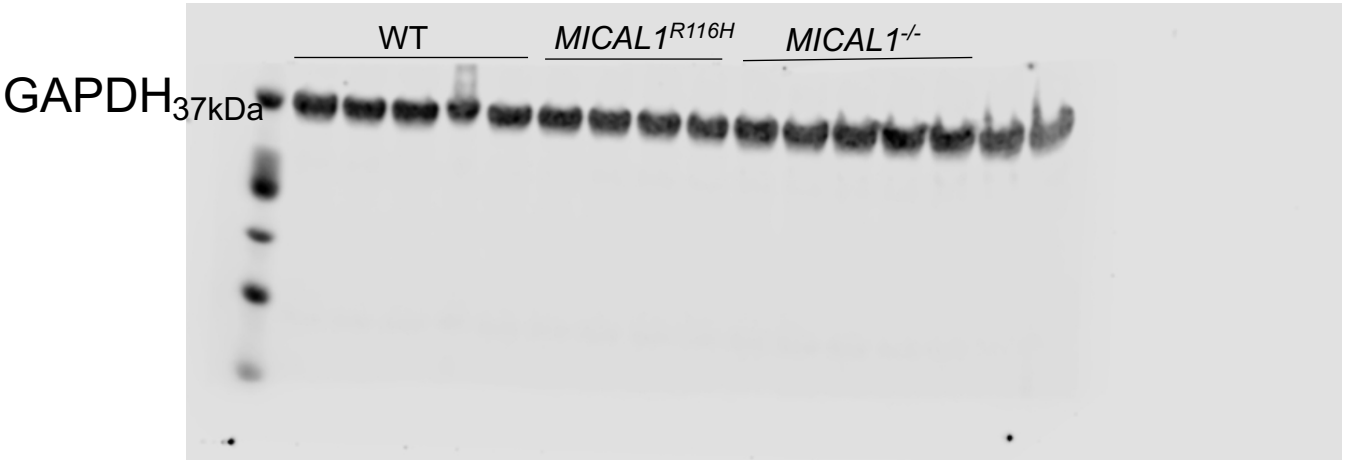
WT
MICAL1R116H
MICAL1-/-
GAPDH37kDa

Figure 2B

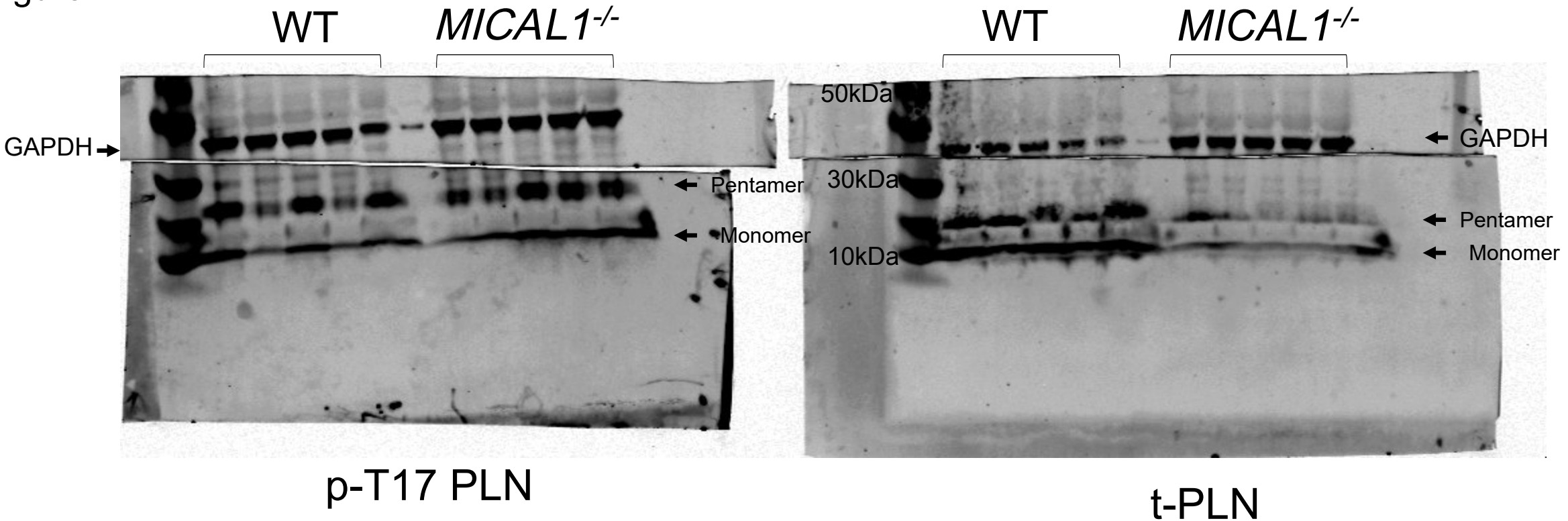
WT
MICAL1-/-
GAPDH
Pentamer
Monomer
p-T17 PLN
WT
MICAL1-/-
50kDa
30kDa
10kDa
GAPDH
Pentamer
Monomer
t-PLN

Figure S2A

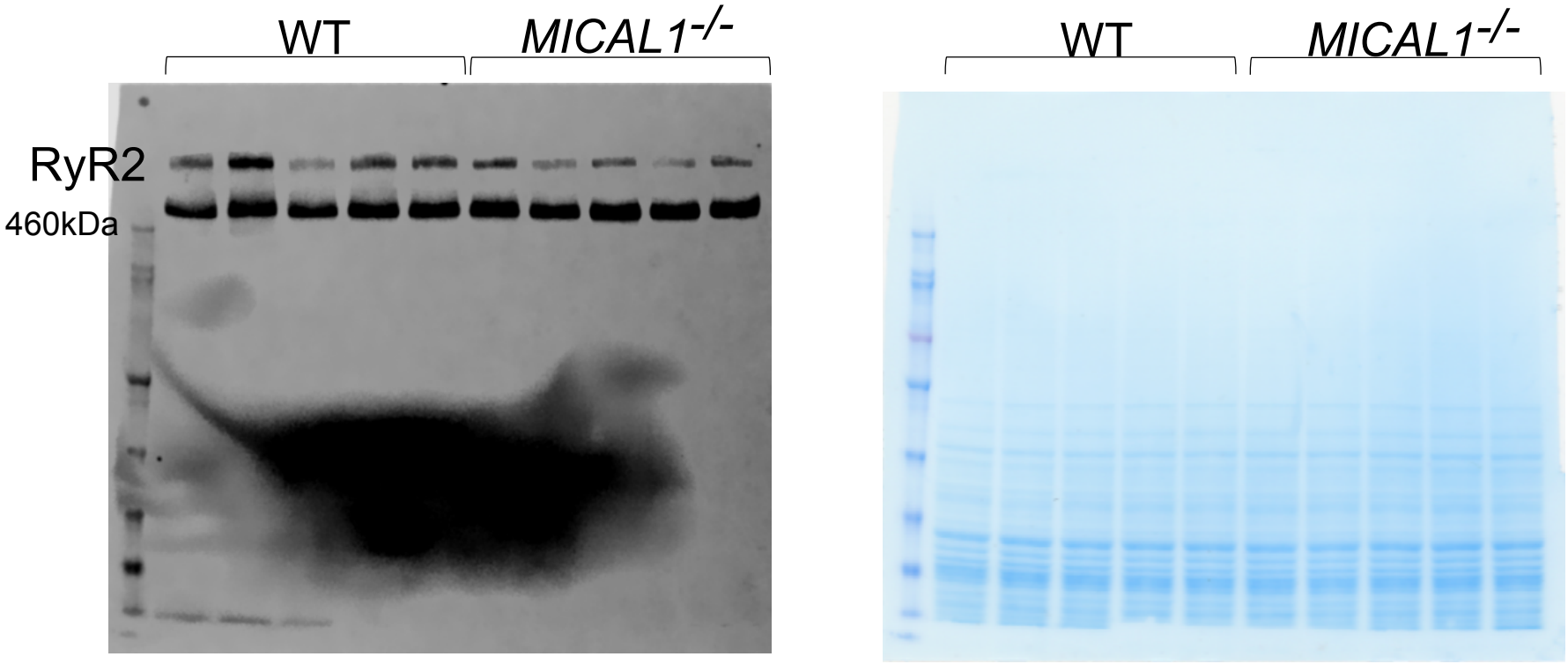

Figure S2B

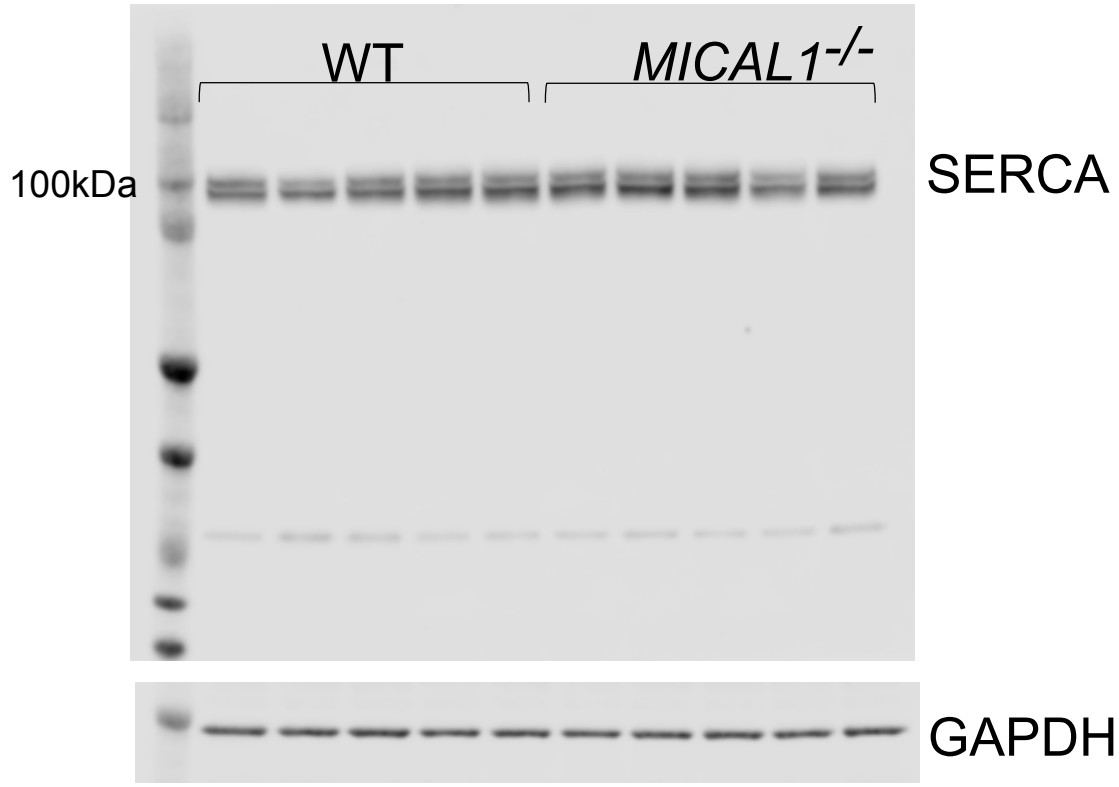

Figure S4D

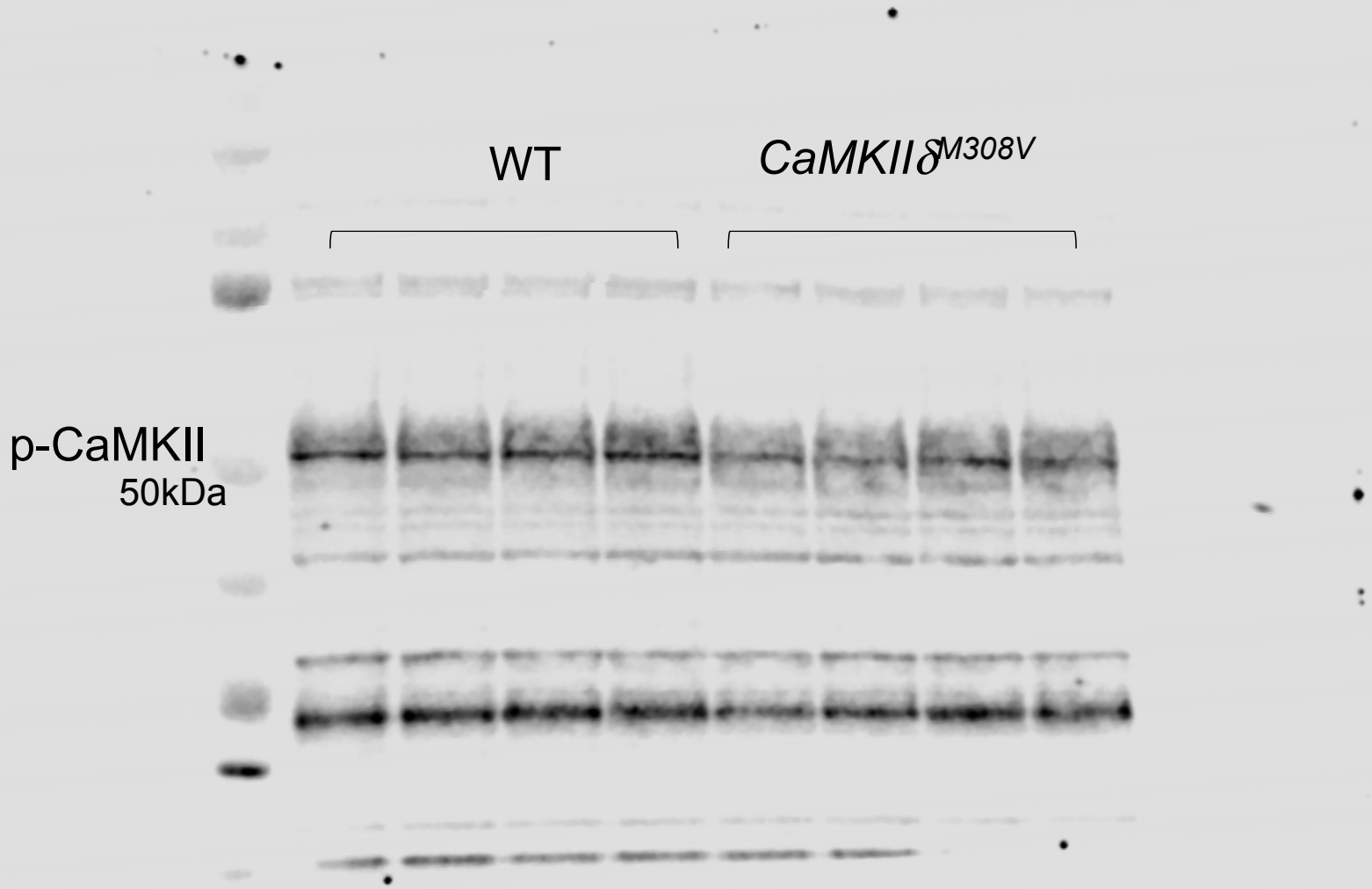

Figure S4D